Modern Physics Letters B
Vol. 35, No. 15 (2021) 2150248 (17 pages)

DOI: 10.1142/S0217984921502481

Numerical investigation on effect of internal flow on vortex-induced vibration dynamics of a full-scale mining riser

Jin-Long Duan*,‡, Xu Wang* and Ke Chen†

*CAS Key Laboratory for Mechanics in Fluid Solid Coupling Systems, Institute of Mechanics, Beijing 100190, China
†State Key Laboratory of Ocean Engineering, Shanghai Jiao Tong University, Shanghai 200240, China
‡duanjl@imech.ac.cn

Received 26 October 2020
Revised 7 December 2020
Accepted 28 December 2020
Published 9 April 2021

The dynamics of a full-scale pipe conveying fluid inside is investigated based on the finite element method (FEM). During the numerical simulation, the Euler–Bernoulli beam equations are used to model the motion of the full-scale pipe while the effect of internal flow is considered. And the semi-empirical time-domain model is applied to simulate the external hydrodynamic forces exerted on the pipe. Then the typical vortex-induced vibration (VIV) characteristics of the full-scale pipe considering both internal and external flows are analyzed. The results show that with the increase of the internal flow velocity, the natural frequencies of the full-scale pipe decrease and the in-line (IL) and cross-flow (CF) dominating modes are increased. Furthermore, the dominating frequencies in both IL and CF directions are not notably changed. And the IL and CF root-mean-square (RMS) values of amplitudes fluctuate at around the stable values due to the stable external hydrodynamic forces. It should be noticed that the IL and CF RMS strain values of the full-scale pipe are increased, especially for high external and internal flow velocities. The maximal RMS strain values in both IL and CF directions appear next to the pipe top, which could have an influence on the motion of the ship on the sea surface.

Keywords: Vortex-induced vibration (VIV) dynamics; full-scale pipe; finite element method (FEM); internal flow.

1. Introduction

A pipe conveying fluid can be encountered in many fields. When the fluid flows inside a pipe, complicated responses occur due to the interaction between the fluid and structures. Such dynamics has been detailed stated in the works of Stangl *et al.*,[1] Wang *et al.*[2] and Kheiri *et al.*[3] In addition, while being exposed to a flowing

‡Corresponding author.

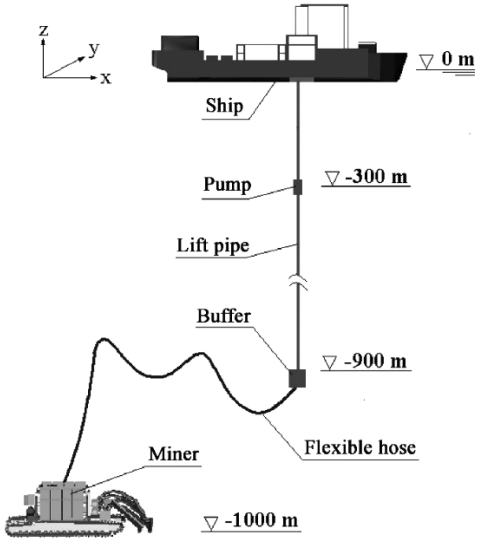

Fig. 1. Sketch of a deep-ocean mining system.[7]

fluid, the pipe conveying internal fluid can be easily subjected to the external excited hydrodynamic forces, which can cause more complicated structural dynamics, as stated by Dai *et al.*[4,5] and Duan *et al.*[6] This phenomenon can be easily found in ocean engineering, especially in deep-sea mining. As shown in Fig. 1, a typical deep-sea mining system is composed of a ship, a lift pipe, a buffer, a flexible hose as well as a miner. After the manganese nodules are collected by the miner from the seafloor, they are vertically transported as two-phase flow to the ship through the pipe system. While the mixture is conveyed, the dynamics of the pipe system is influenced by both the internal and external flows. As a result, more complicated dynamical behavior can be found in the pipe system, especially in lift pipe due to its large length. Therefore, the dynamics of the pipe system used in deep-sea mining industry has drawn much attention for decades. Correspondingly, many academic achievements are found in this field, the details of which can be found in Refs. 7–10.

Among these studies, experiments have been conducted to investigate the dynamics of pipes subjected to external fluid. Feng[11] and Khalak and Williamson[12] experimentally studied the dynamics of risers with high and low mass damping, respectively. Typical characteristics of vortex-induced vibration (VIV) were analyzed, such as the vibrating amplitudes, frequency as well as the response branches. Trim *et al.*[13] carried out an experiment in order to research the VIV dynamics of a long slender riser. They found that multi-mode responses occurred under different flow velocities and the damage fatigue could be largely affected by the vibrating amplitudes. Song *et al.*[14,15] investigated the hydrodynamics on a slender riser by conducting an experiment. The hydrodynamic coefficients were focused while the in-line (IL) and cross-flow (CF) motions of the riser were considered. In addition,

a model was proposed based on their experimental data. Apart from these studies, more experimental investigations on risers subjected to external flow can be also found in the works of Raghavan and Bernitsas,[16] Bourdier and Chaplin,[17] Srinil *et al.*,[18] Goncalves *et al.*[19] and Gao *et al.*[20]

Although the experimental method is the best way to investigate the dynamics of a slender pipe, there exists limitation of experiments, such as the inaccuracy of the experimental conditions. Therefore, numerical simulation has been widely applied to study the VIV of flexible pipes. Computational Fluid Dynamics (CFD) and semi-empirical method are commonly used by many researchers during the numerical simulation of VIV. Based on the discrete vortex method, Yamamoto *et al.*[21] proposed a quasi-three-dimensional (3D) model in order to research the dynamical behavior and the hydrodynamic forces of an oscillating flexible cylinder. Evangelinos *et al.*[22] studied the hydrodynamic forces on a flexible cylinder by using the direct numerical simulation (DNS). Thorsen *et al.*[23,24] developed a semi-empirical time-domain method to investigate the VIV dynamics of a slender riser subjected to uniform and shear flows. The numerical results, such as response mode, vibrating frequency and damage fatigue, show a great agreement with the experimental data. Besides, plenty of studies are also carried out to study the VIV dynamics of flexible risers numerically, see Refs. 25–27.

However, all the aforesaid studies were mainly focusing on the dynamics of pipes considering external flow. It has been proved that the internal flow also has an important effect on the dynamics of the pipe by Wang,[28] Modarres-Sadeghi and Païdoussis[29] and Kheiri and Païdoussis.[30] Dai and Wang[31] used the multiple scales method to study the influence of internal flow on the dynamics of the pipe conveying fluid. Then, Dai *et al.*[10] studied the VIV dynamics of a pipe considering the internal flow velocities in the subcritical and supercritical regimes. More complicated responses are found during their simulation. Recently, Duan *et al.*[32] focused on the VIV dynamics of a slender riser considering both internal and external flows. The mode responses are found to be closely related to the internal flow velocity. Additionally, some researches focusing on the VIV dynamics of pipe transporting fluid can be also found, see Refs. 33–35 for more details. Although the dynamics of pipes with internal and external flows has been researched, most of the studies were focusing on the dynamics of scaled pipes. Few papers can be found for the full-scale pipe considering both the internal and external flows. However, there exists a discrepancy in accuracy of the results between full-scale and scaled models. Therefore, it is necessary to study the dynamics of the deep-ocean pipe coupling both internal and external flows by focusing on a full-scale model. Hence, the main objective of this study is to investigate the three-dimensional dynamics of a full-scale pipe subjected to both internal and external flows so that the dynamical behavior of the pipe system for deep-sea mining can be understood more comprehensively.

In this paper, the Euler–Bernoulli beam equations considering the effect of internal flow and the semi-empirical time-domain model by Thorsen *et al.*,[23,24] are introduced and applied. And the full-scale pipe from the report of China's 1000-m

deep-ocean poly-metallic nodule mining pipeline system is modeled. Then the VIV dynamics of the full-scale pipe considering both internal and external flows is analyzed and discussed. Typical VIV dynamics, such as the response amplitudes, dominating modes and frequencies as well as the root-mean-square (RMS) values of strains, are mainly focused.

2. Analytical Model and Method for the Lift Pipe

2.1. *Governing equations of motion*

The pipe system for deep-sea mining, which consists of a lift pipe, a buffer and a flexible hose which can be of length up to several thousand meters, is shown in Fig. 1. Since the length of the lift pipe almost accounts for the whole length of the pipe system, it is important to focus on the dynamics of the lift pipe. Therefore, the VIV dynamics of the full-scale lift pipe considering both the internal and external flows is investigated in this study, as shown in Fig. 2. As the external flow velocity is less than 1 m/s, the ship and the buffer are assumed static in order to simplify the model during the numerical simulation (Fig. 2). Hence, the motion of the ship, buffer and pump is ignored during our study. Moreover, gravity, buoyancy, internal damping and pressurization effects are not taken into account. According to Ref. 36, the governing equations of motion are expressed as follows:

$$m\frac{\partial^2 x(z,t)}{\partial t^2} + c\frac{\partial x(z,t)}{\partial t} + 2m_f U_i \frac{\partial^2 x(z,t)}{\partial z \partial t} + (m_f U_i^2 - T)\frac{\partial^2 x(z,t)}{\partial z^2} + \mathrm{EI}\frac{\partial^4 x(z,t)}{\partial z^4} = f_x(z,t), \tag{1}$$

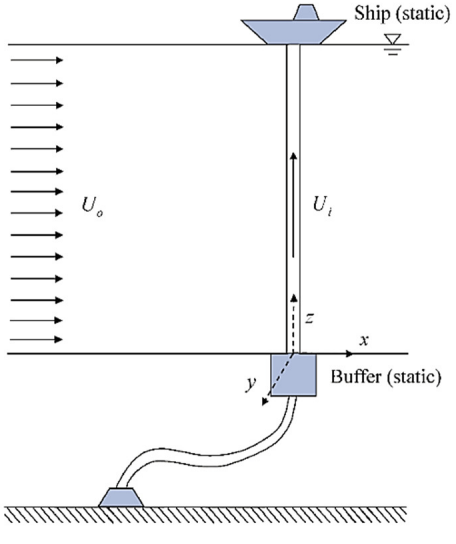

Fig. 2. (Color online) The model of a deep-ocean mining system.

$$m\frac{\partial^2 y(z,t)}{\partial t^2} + c\frac{\partial y(z,t)}{\partial t} + 2m_f U_i \frac{\partial^2 y(z,t)}{\partial z \partial t} + (m_f U_i^2 - T)\frac{\partial^2 y(z,t)}{\partial z^2} + \mathrm{EI}\frac{\partial^4 y(z,t)}{\partial z^4} = f_y(z,t), \tag{2}$$

where $x(z,t)$ and $y(z,t)$ are the dimensional displacements in the IL and CF directions, respectively, m is the mass (including the pipe mass, the internal fluid mass and the additional fluid mass), EI is the flexural stiffness, L is the pipe length, U_i is the internal flow velocity, m_f is the internal fluid mass, c is the structure damping and T is the pretension force. $f_x(z,t)$ and $f_y(z,t)$ are the hydrodynamic forces caused by the external flow in the IL and CF directions.

2.2. *External hydrodynamic forces*

Dynamic excitation considered during the simulation includes the external hydrodynamic forces that are caused by the ocean current. The hydrodynamic force consists of the excitation force, the damping force and the added mass force. The details are provided in the works of Thorsen *et al.*,[23,24]

$$f_x = \frac{1}{4}\rho_o D C_\nu U_o \dot{y}_0 \cos\phi_{\mathrm{exc},x} - \frac{1}{2}\rho_o D C_{x1} U_o \dot{x} - \frac{1}{2}\rho_o A_x C_{x2} |\dot{x}\,|\,\dot{x} - \frac{\rho_o \pi D^2}{4} C_{ax}\ddot{x}\,, \tag{3}$$

$$f_y = \frac{1}{2}\rho_o D C_\nu U_o^2 \cos\phi_{\mathrm{exc},y} - \frac{1}{2}\rho_o D C_{y1} U_o \dot{y} - \frac{1}{2}\rho_o A_y C_{y2} |\dot{y}\,|\,\dot{y} - \frac{\rho_o \pi D^2}{4} C_{ay}\ddot{y}\,, \tag{4}$$

where the excitation force, the damping force and the added mass force are contained. In these equations, ρ_o is the external fluid density, D is the external diameter and C_v is an empirical coefficient related to the CF vibration amplitude A_y. A_x and A_y are the IL and CF vibrating amplitudes. $\phi_{\mathrm{exc},x}$ and $\phi_{\mathrm{exc},y}$ are the instantaneous phases of the IL and CF forces. C_{x1}, C_{x2}, C_{y1} and C_{y2} are the damping coefficients. In addition, $C_{x1} = 0.507$, $C_{x2} = 0.936$, $C_{y1} = 0.485$, $C_{y2} = 0.936$ and $C_{ax} = C_{ay} = 1$ are adopted here according to Ref. 24.

2.3. *The full-scale pipe model*

In order to investigate the dynamics of the full-scale pipe considering both internal and external flows, a 900-m-long pipe is chosen according to Li *et al.*[7] The prototype of the pipe is from the report of China's 1000-m deep-ocean poly-metallic nodule mining pipeline system. The properties of the lift pipe are presented in Table 1.

As the biggest external flow velocity in the south ocean of China is 0.772 m/s according to Li *et al.*,[7] the biggest flow velocity is set to 1 m/s during our simulation. Although the manganese nodules are transported in the lift pipe, the internal flow

Table 1. The characteristics of the pipe model.

Parameter	Value
Length (L)	900 m
External diameter (D)	0.219 m
Internal diameter (d)	0.2063 m
Axial tension (T)	2.22×10^5 N
Young's modulus of elasticity (E)	2.06×10^{11} N/m^2
Pipe mass per meter (m)	56.9 kg

is considered as uniform flow in order to simplify the model. And the internal flow density is set up to 2000 kg/m^3.

2.4. *Numerical method*

The finite element method (FEM) is used to discretize the governing equations first. Here, we have the following equation:

$$\mathbf{M}\ddot{\mathbf{d}}(t) + \mathbf{C}\dot{\mathbf{d}}(t) + \mathbf{K}\mathbf{d}(t) = \mathbf{F}(t), \tag{5}$$

where $\mathbf{d}(t)$ and $\mathbf{F}(t)$ are the nodal displacement and force vectors, $\mathbf{M}$ is the mass matrix, $\mathbf{C}$ is the damping matrix and $\mathbf{K}$ is the stiffness matrix. In addition, $\mathbf{C} = \alpha_1\mathbf{M} + \alpha_2\mathbf{K}$, where $\alpha_1 = 10^{-2}$ and $\alpha_2 = 10^{-4}$ are taken into account according to Thorsen *et al.*[24]

There are several kinds of integration schemes that can be used for solving the discretized equations. Among these methods, the Newmark scheme is effective and adopted, as it was in the previous papers as well. The Newmark-β method is with $\gamma = 0.5$ and $\beta = 0.25$.

Before the calculation, the required number of time steps needs to be determined. Here, the time history of the pipe mid-point is calculated with three time

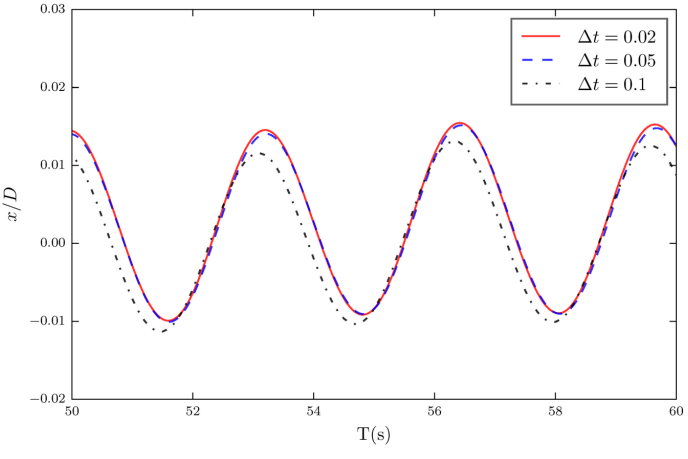

Fig. 3. (Color online) The time history of IL displacement of the pipe mid-point with different time steps.

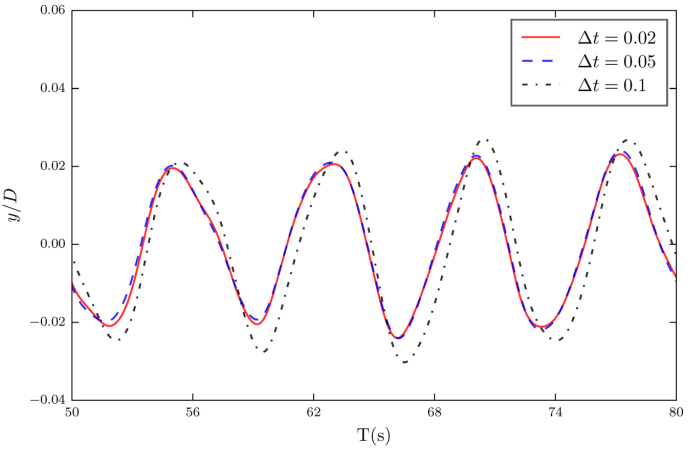

Fig. 4. (Color online) The time trace of CF displacement of the pipe mid-point with different time steps.

steps (0.1, 0.05 and 0.02). And the IL and CF displacements of the pipe mid-point are plotted versus time in Figs. 3 and 4. These comparisons show that the dynamic responses of the full-scale pipe can be predicted reasonably accurately if $\Delta t = 0.05$. Therefore, the time step of 0.05 is used in our study.

3. Results and Discussion

The numerical results predicted by this semi-empirical model have been compared with the experimental data by Thorsen *et al.*[24] and Duan *et al.*,[32] which proved the accuracy of this model. Therefore, the semi-empirical model is utilized to investigate the dynamics of the lift pipe while the manganese nodules are transported. And some typical VIV characteristics, such as the dominating mode and frequency as well as the IL and CF RMS amplitudes, are mainly analyzed. Here, the lift pipe under five external velocities (0.2, 0.4, 0.6, 0.8 and 1 m/s) and 10 internal velocities (from 5 m/s to 50 m/s with increment of 5 m/s) is studied.

The initial values of structure displacements, velocities and accelerations at the beginning of the calculation are set to 0.00001. The initial values of phases are independent random values between 0 and 2π according to Thorsen *et al.*[24]

3.1. *Natural frequency of the lift pipe with internal flow*

First, the natural frequency f_n of the lift pipe considering both the internal and external flows is focused. The variation of natural frequency of the lift pipe conveying fluid is depicted in Fig. 5. Since it is difficult to demonstrate each mode frequency of the pipe, only the first three mode frequencies f_n are shown in Fig. 5. As seen in this figure, the natural frequencies for all three modes decrease with the increase of the internal flow velocities, which is similar to the conclusion of Guo and Lou.[37] When the fluid in the pipe is static, the natural frequencies f_n for the first, second

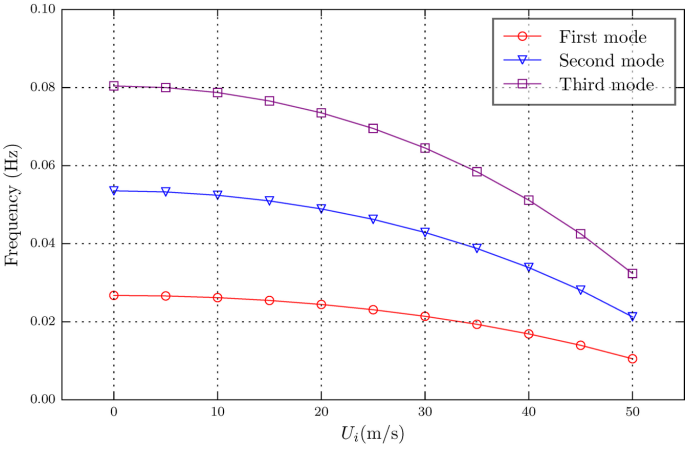

Fig. 5. (Color online) The first three natural frequencies of the pipe with increasing internal fluid velocity.

and third modes are 0.0268, 0.0536 and 0.0804 Hz, respectively. However, while the internal flow velocity U_i is increased up to 50 m/s, the first, second and third mode frequencies decrease to 0.0105, 0.0213 and 0.0324 Hz (Fig. 5). Such change can be attributed to the decrease of the structural stiffness due to the existence of the internal flow. Moreover, the decrease of the natural frequency can lead to more complicated dynamics of the pipe.

3.2. *IL and CF dominating modes and frequencies*

With the increase of the internal flow velocity, the dominating modes in both IL and CF directions under different internal and external flow velocities are illustrated in Figs. 6 and 7. Obviously, the IL and CF dominating modes increase with the increase of the internal flow velocities U_i for all the external flow velocities U_o. As seen in Figs. 6 and 7, the IL and CF dominating modes of the pipe with $U_i = 5$ m/s and $U_o = 0.4$ m/s are 20 and 11, respectively. When U_i increases to 50 m/s, the dominating modes in IL and CF directions are 27 and 18. It should be also noted that the IL dominating modes are almost twice as much as those in the CF direction while the internal and external flow velocities are relatively low. However, with the increase of U_i, this phenomenon disappears. For example, when $U_i = 50$ m/s and $U_o = 1$ m/s, the IL dominating mode is 48 while the one dominating in CF direction is 32. The increase of the IL and CF dominating modes can be attributed to the decrease of the riser natural frequency due to the increase of the internal flow velocity. As the natural frequencies f_n of the pipe are decreased, the frequency of the external hydrodynamic force tends to lock onto the new decreased natural frequency. As a result, higher mode vibrations could be excited more easily. Therefore, higher IL and CF modes are detected in our study with the increase of U_i.

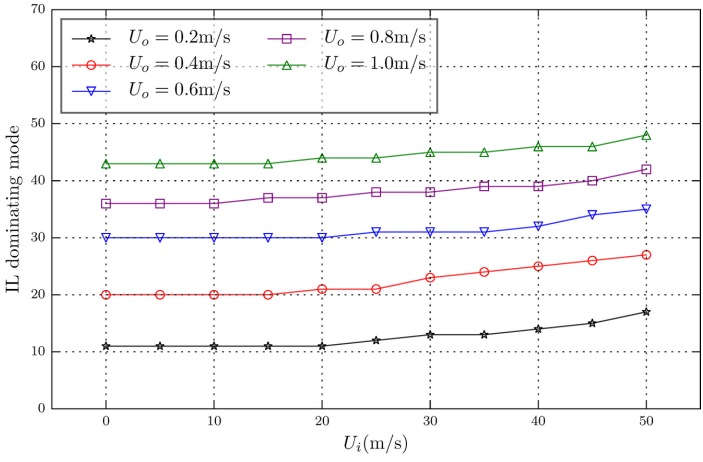

Fig. 6. (Color online) IL dominating modes of the pipe considering internal flow.

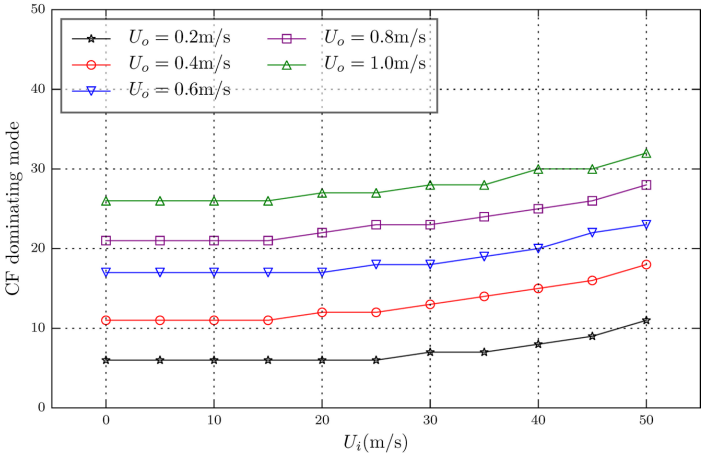

Fig. 7. (Color online) CF dominating modes of the pipe considering internal flow.

In addition, it should be noticed that the IL and CF dominating modes stay stable when the internal flow velocities U_i are at relatively low values. The reason for this phenomenon is that the IL and CF dominating modes are mainly influenced by the external flow when the values of U_i are low. Then the IL and CF dominating modes begin to increase at a certain internal velocity while U_i is increased. As shown in Figs. 6 and 7, the critical value of the internal flow velocity under different external flow velocities U_o is between 15 m/s and 25 m/s when the dominating modes start to increase in our study. While U_i is beyond the critical values, the IL and CF dominating modes increase evidently. And the maximal dominating modes for both responses appear at 50 m/s during our simulation. Take the case $U_o = 0.4$ m/s as an example. The IL and CF dominating modes are 20 and 11,

Table 2. The IL dominating frequency f_{ex} of the pipe considering internal flow.

Cases	External flow velocity U_o (m/s)					
	0.4			0.8		
Internal flow velocity U_i (m/s)	Dominating mode	f_n corresponding to dominating mode	f_{ex}	Dominating mode	f_n corresponding to dominating mode	f_{ex}
0	20	0.5858	0.594	36	1.2353	1.226
5	20	0.5838	0.592	36	1.2329	1.222
10	20	0.5779	0.582	36	1.2258	1.216
15	20	0.5678	0.594	37	1.2622	1.250
20	21	0.5876	0.604	37	1.2456	1.232
25	21	0.5690	0.584	38	1.2732	1.256
30	23	0.6148	0.608	38	1.2469	1.228
35	24	0.6220	0.614	39	1.2655	1.240
40	25	0.6248	0.616	39	1.2294	1.228
45	26	0.6231	0.610	40	1.2390	1.230
50	27	0.6170	0.622	42	1.2971	1.280

Table 3. The CF dominating frequency f_{ey} of the pipe considering internal flow.

Cases	External flow velocity U_o (m/s)					
	0.4			0.8		
Internal flow velocity U_i (m/s)	Dominating mode	f_n corresponding to dominating mode	f_{ey}	Dominating mode	f_n corresponding to dominating mode	f_{ey}
0	11	0.3030	0.302	21	0.6203	0.618
5	11	0.3016	0.300	21	0.6183	0.616
10	11	0.2974	0.298	21	0.6122	0.612
15	11	0.2905	0.296	21	0.6020	0.613
20	12	0.3085	0.304	22	0.6222	0.618
25	12	0.2948	0.296	23	0.6033	0.630
30	13	0.3046	0.302	23	0.6148	0.614
35	14	0.3096	0.306	24	0.6220	0.618
40	15	0.3094	0.306	25	0.6248	0.622
45	16	0.3039	0.302	26	0.6231	0.620
50	18	0.3204	0.316	28	0.6551	0.644

respectively, when the internal fluid is static. While the internal flow velocity U_i increases to 5, 10 and 15 m/s, the dominating modes in both IL and CF directions are still 20 and 11. At $U_i = 20$ m/s, the IL and CF dominating modes start to increase. And the maximal values appear when $U_i = 50$ m/s for both IL and CF responses.

The IL and CF dominating frequencies of the pipe with $U_o = 0.4$ m/s and 0.8 m/s are demonstrated in Tables 2 and 3. The results show that the IL and CF dominating frequencies are almost stable with the increase of the internal flow velocities. For example, when $U_o = 0.4$ m/s, the IL and CF dominating frequencies

fluctuate at around 0.6 Hz and 0.3 Hz, respectively. The reason for this phenomenon is that the vortex shedding frequencies almost keep stable during this investigation. Moreover, the decrease of the natural frequency is not notable with the increase of the internal flow velocity. Even if the frequency of the external hydrodynamic force is locked onto the new decreased natural frequency, the IL and CF dominating frequencies are not changed evidently. This phenomenon can also be found in Ref. 32. The IL and CF frequencies remain almost stable during the above study. As high mode vibration of pipes can lead to high damage fatigue, more attention should be paid to the dynamics of pipe conveying flows inside.

3.3. *RMS values of IL and CF amplitudes and strains*

The RMS values of IL and CF amplitudes are illustrated in Figs. 8 and 9. It is obvious that with the increase of the internal flow velocities U_i for a constant external flow velocity U_o, the RMS values of amplitudes in both IL and CF directions almost fluctuate at around the stable values. For example, the values of IL RMS amplitudes fluctuate at around 0.01 and 0.09 when the external flow velocities U_o are 0.2 m/s and 1 m/s, respectively. Likewise, the RMS amplitudes in CF direction fluctuate at around 0.15 and 0.45 when $U_o = 0.2$ m/s and 1 m/s, respectively. The main reason is that the external fluid forces being exerted on the lift pipe play a dominate role during the calculation, which causes the dominating IL and CF responses to be mainly influenced by external flow. As a result, the effect of internal flow on the IL and CF RMS amplitudes is not evident in our study. Since the external fluid forces mainly determine the values of the amplitudes, the RMS values of the amplitudes in both IL and CF directions fluctuate at around stable values under different internal flow velocities.

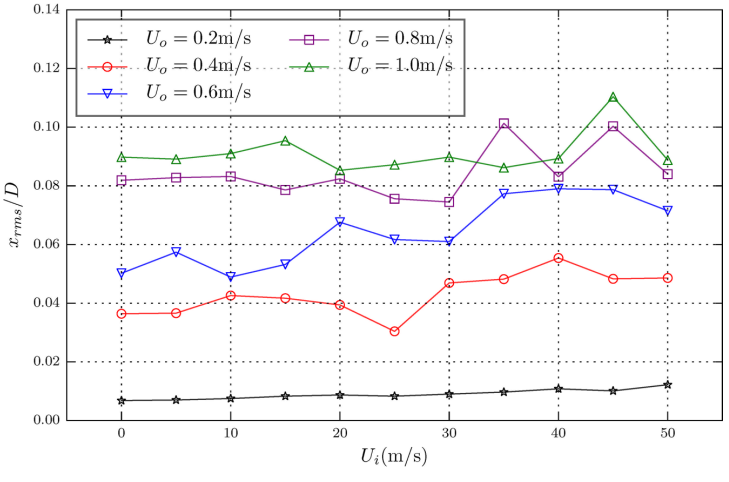

Fig. 8. (Color online) IL RMS amplitudes of the pipe considering internal flow.

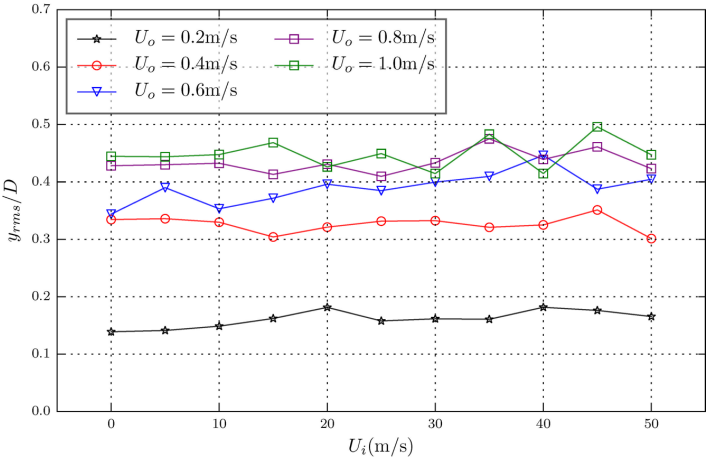

Fig. 9. (Color online) CF RMS amplitudes of the pipe considering internal flow.

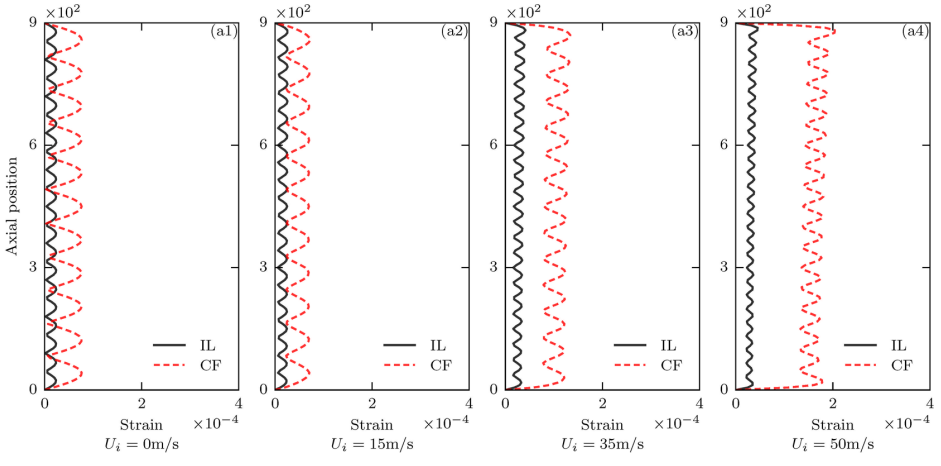

Fig. 10. (Color online) IL and CF RMS strain values of the pipe with different internal flow velocities ($U_o = 0.4$ m/s).

Figures 10–12 illustrate the IL and CF strains of the pipe with different internal flow velocities U_i while the external flow velocities U_o are 0.4, 0.8 and 1 m/s. It can be seen from the figures that when the fluid in the pipe is static, the maximal values of IL and CF strains are stable along the pipe for all the external flow velocities. When $U_o = 0.4$, 0.8 and 1 m/s, the IL RMS values of strains are approximately 0.2×10^{-4}, 2×10^{-4} and 2.5×10^{-4} and the RMS values of strains in the CF direction are about 0.8×10^{-4}, 3.8×10^{-4} and 5.5×10^{-4}. While the fluid in the pipe begins to flow, the strains of the pipe change in both IL and CF directions along its axial position. With the increase of the internal flow velocity U_i, this phenomenon is more obvious, as shown in Figs. 10–12. The IL and CF strains of the pipe bottom

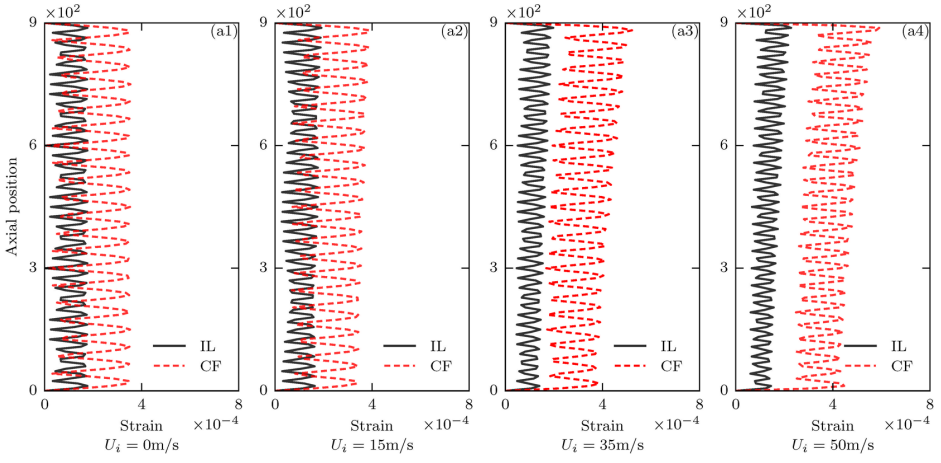

Fig. 11. (Color online) IL and CF RMS strain values of the pipe with different internal flow velocities ($U_o = 0.8$ m/s).

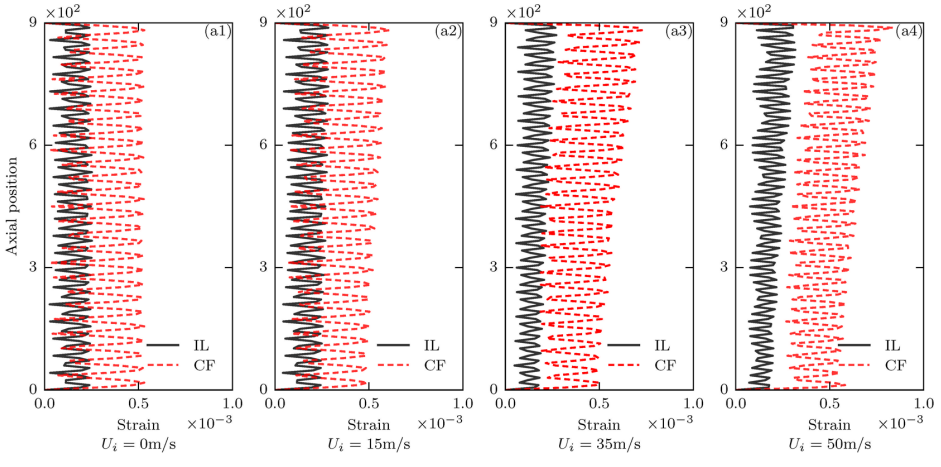

Fig. 12. (Color online) IL and CF RMS strain values of the pipe with different internal flow velocities ($U_o = 1$ m/s).

are almost stable with the increase of U_i. However, the RMS values of IL and CF strains of the pipe top are evidently increased, especially for high values of external flow velocities U_o. During our study, while $U_o = 0.8$ m/s and 1 m/s, the maximal CF strain values of the pipe top are up to approximately 6×10^{-4} and 8.5×10^{-4}. The reason for this change is that with high U_i, the influence of the interaction between the internal fluid and the pipe is more evident. As a consequence, the internal force exerted on the pipe plays an unignorable role in VIV, which leads to the change of VIV characteristics, especially for high external flow velocity. Since the pipe top connects to the ship on the sea surface, the effect of internal flow on the strains of the pipe should not be ignored in ocean engineering.

3.4. *VIV dynamics considering different internal fluid densities*

The VIV characteristics of a full-scale pipe conveying internal flow with different densities under $U_o = 0.8$ m/s are presented in Tables 4 and 5. The change of the IL and CF dominating modes with the increase of the internal fluid density is similar to that with the increase of the internal flow velocity. It can be seen that both the IL and CF dominating modes increase while the internal fluid density is increased. But it should be noted that when the internal fluid density is high, the internal flow velocity at which mode transition occurs for IL and CF responses is lower. As is observed in Tables 4 and 5, when $\rho_i = 1000$ kg/m^3, mode transition occurs with the internal flow velocity U_i equal to 20 m/s for both IL and CF responses. But the internal flow velocity is 10 m/s when mode transition appears in IL and CF directions with $\rho_i = 3000$ kg/m^3. This can be attributed to that the internal fluid density also has an effect on the pipe stiffness, leading to mode transition in IL and CF directions.

As for the IL and CF RMS amplitudes and dominating frequencies, no obvious change is observed. It can be seen from Tables 4 and 5 that IL and CF RMS

Table 4. IL VIV responses of the pipe considering different internal fluid densities.

Cases	Internal fluid density ρ_i (kg/m^3)								
	1000			2000			3000		
U_i(m/s)	Mode	f_{ex}	RMS	Mode	f_{ex}	RMS	Mode	f_{ex}	RMS
5	36	1.224	0.0823	36	1.222	0.0828	36	1.222	0.0829
10	36	1.270	0.0658	36	1.216	0.0832	37	1.258	0.0760
15	36	1.264	0.0713	37	1.250	0.0768	37	1.238	0.0806
20	37	1.254	0.0750	37	1.232	0.0824	38	1.258	0.0735
25	37	1.242	0.0799	38	1.256	0.0756	39	1.272	0.0757
30	37	1.228	0.0867	38	1.228	0.0745	39	1.254	0.0771
35	38	1.260	0.0748	39	1.240	0.1013	40	1.252	0.0816
40	38	1.238	0.0808	39	1.228	0.0831	41	1.296	0.0838

Table 5. CF VIV responses of the pipe considering different internal fluid densities.

Cases	Internal flow density ρ_i (kg/m^3)								
	1000			2000			3000		
U_i(m/s)	Mode	f_{ey}	RMS	Mode	f_{ey}	RMS	Mode	f_{ey}	RMS
5	21	0.618	0.4290	21	0.616	0.4300	21	0.616	0.4314
10	21	0.642	0.3833	21	0.612	0.4325	22	0.634	0.4031
15	21	0.638	0.3933	22	0.613	0.4131	23	0.622	0.4279
20	22	0.632	0.4049	22	0.618	0.4309	23	0.630	0.4145
25	22	0.626	0.4210	23	0.630	0.4097	25	0.634	0.4315
30	22	0.618	0.4399	23	0.614	0.4332	26	0.634	0.4129
35	23	0.634	0.4043	24	0.618	0.4751	28	0.628	0.4460
40	23	0.622	0.4293	25	0.622	0.4392	29	0.648	0.4155

amplitudes and dominating frequencies fluctuate at around stable values at certain internal fluid densities. This phenomenon can be attributed to that the external hydrodynamic forces mainly account for the IL and CF RMS amplitudes. As the external flow velocity is not changed, the external hydrodynamic force is stable during our simulation.

4. Conclusions

In this paper, the dynamical behavior of a full-scale lift pipe considering both internal and external flows is studied. The Euler–Bernoulli beam equations considering the effect of internal flow are discretized by using FEM. Then the governing equations are solved based on the Newmark-β method. And the external hydrodynamic forces are simulated by using the semi-empirical time-domain model. Some dynamic characteristics of the full-scale pipe, such as the natural frequencies, the IL and CF dominating modes and frequencies as well as the RMS values of amplitudes and strains in IL and CF directions, are mainly focused under different internal and external flow velocities and densities. The main conclusions are drawn as follows:

(1) The natural frequencies of the full-scale pipe with internal flow are obviously influenced by the internal flow velocity. With the increase of the internal flow velocity, the natural frequencies of the full-scale pipe decrease evidently.
(2) When the internal flow velocity is increased under a constant external flow velocity, the IL and CF dominating modes of the pipe conveying fluid inside increase due to the decrease of the natural frequencies. And the maximal modes in IL and CF directions appear at the highest values of internal flow velocity.
(3) The IL and CF dominating frequencies almost keep stable with the increase of the internal flow velocity under a constant external flow velocity as the natural frequencies are not changed notably. The RMS values of amplitudes in IL and CF directions almost fluctuate at around stable values due to the stable external hydrodynamic forces.
(4) The IL and CF RMS values of strains of the full-scale pipe are influenced by the internal fluid, especially when the internal and external flow velocities are high. The IL and CF RMS strain values are increased with the increase of the internal flow velocity. The maximal values of the RMS strain in IL and CF directions appear at the pipe top with high internal and external flow velocities.
(5) When the internal fluid density is increased, mode transition is observed with low internal flow velocity for high internal fluid density. But the IL and CF RMS amplitudes and dominating frequencies are almost stable regardless of the internal fluid density.

Since the environmental conditions are more complicated in ocean engineering, more investigations, such as experiments, should be performed in order to study the dynamical behavior of pipes transporting fluid inside and provide a thorough

understanding of VIV mechanism of such pipes. It will be of great significance for the deep-sea mining industry.

Acknowledgments

The authors acknowledge the supports of the National Key R&D Program of China (2017YFC1404200), National Natural Science Foundation of China (Grants 11572332 and 11972352) and the Strategic Priority Research Program of the Chinese Academy of Sciences (Grants XDB22040203 and XDA22000000).

References

1. M. Stangl, J. Gerstmayr and H. Irschik, *J. Sound Vib.* **310** (2008) 493.
2. L. Wang, H. L. Dai and Q. Qian, *J. Fluid Struct.* **29** (2012) 97.
3. M. Kheiri, M. P. Païdoussis, G. C. Del Pozo and M. Amabili, *J. Fluid Struct.* **49** (2014) 360.
4. H. L. Dai, L. Wang, Q. Qian and Q. Ni, *J. Fluid Struct.* **39** (2013) 322.
5. H. L. Dai, L. Wang, Q. Qian and Q. Ni, *Ocean Eng.* **77** (2014) 12.
6. J. L. Duan, K. Chen, Y. X. You and J. L. Li, *Appl. Ocean Res.* **72** (2018) 110.
7. Y. Li, S. J. Liu and L. Li, *China Ocean Eng.* **21** (2007) 175.
8. Y. Dai and S. J. Liu, *China Ocean Eng.* **27** (2013) 231.
9. S. D. Hannot and J. M. van Wijk, Heave induced internal flow fluctuations in vertical transport systems for deep ocean mining, in *Proc. ASME 2014 33rd Int. Conf. Ocean, Offshore and Arctic Engineering*, Vol. 8A: Ocean Engineering (American Society of Mechanical Engineers, 2014).
10. Y. Dai, H. Liu, T. Zhang, S. J. Liu and Y. Li, *Teh. Vjesn. (Tech. Gazette)* **23** (2016).
11. C. Feng, The measurement of vortex induced effects in flow past stationary and oscillating circular and d-section cylinders, M.Sc. thesis, University of British Columbia (1968).
12. A. Khalak and C. H. K. Williamson, *J. Fluid Struct.* **10** (1996) 455.
13. A. D. Trim, H. Braaten, H. Lie and M. A. Tognarelli, *J. Fluid Struct.* **21** (2005) 335.
14. L. Song, S. Fu, J. Cao, L. Ma and J. Wu, *J. Fluid Struct.* **63** (2016) 325.
15. L. Song, S. Fu, Y. Zeng and Y. Chen, *J. Waterw. Port Coast. Ocean Eng.* **142** (2016) 04016001.
16. K. Raghavan and M. M. Bernitsas, *Ocean Eng.* **38** (2011) 719.
17. S. Bourdier and J. R. Chaplin, *J. Fluid Struct.* **29** (2012) 62.
18. N. Srinil, H. Zanganeh and A. Day, *Ocean Eng.* **73** (2013) 179.
19. R. T. Goncalves, G. F. Rosetti, G. R. Franzini, J. R. Meneghini and A. L. C. Fujarra, *J. Fluid Struct.* **39** (2013) 237.
20. Y. Gao, J. Yang, Y. Xiong, M. Wang and G. Peng, *Appl. Ocean Res.* **59** (2016) 53.
21. C. T. Yamamoto, J. R. Meneghini, F. Saltara, R. A. Fregonesi and J. A. Ferrari, Jr., *J. Fluid Struct.* **19** (2004) 467.
22. C. Evangelinos, D. Lucor and G. E. Karniadakis, *J. Fluid Struct.* **14** (2000) 429.
23. M. J. Thorsen, S. Sævik and C. M. Larsen, *J. Fluid Struct.* **49** (2014) 135.
24. M. J. Thorsen, S. Sævik and C. M. Larsen, *Mar. Struct.* **41** (2015) 200.
25. M. M. Zhang, S. X. Fu, H. J. Ren, R. Li and L. J. Song, A time domain prediction method for vortex-induced vibrations of a flexible pipe with time-varying tension, in *Proc. ASME 2018 37th Int. Conf. Ocean, Offshore and Arctic Engineering* (American Society of Mechanical Engineers, 2018).

26. Z. Q. Lu, M. M. Zhang, S. X. Fu and H. J. Ren, *Mar. Struct.* **64** (2019) 492.
27. Y. Qu and A. V. Metrikine, *Ocean Eng.* **196** (2020) 106732.
28. L. Wang, *Int. J. Non-Linear Mech.* **44** (2009) 115.
29. Y. Modarres-Sadeghi and M. P. Païdoussis, *Comput. Struct.* **22** (2013) 192.
30. M. Kheiri and M. P. Païdoussis, *J. Fluid Struct.* **55** (2015) 204.
31. H. L. Dai and L. Wang, *Theor. Appl. Mech. Lett.* **2** (2012) 022006.
32. J. L. Duan, K. Chen, Y. X. You, R. F. Wang and J. L. Li, *Int. J. Nav. Archit. Ocean Eng.* **10** (2018) 692.
33. L. Wang, T. L. Jiang, H. L. Dai and Q. Ni, *J. Sound Vib.* **422** (2018) 590.
34. W. Yang, Z. Ai, X. Zhang, X. Chang and R. Gou, *Int. J. Mech. Sci.* **138** (2018) 99.
35. T. L. Jiang, Z. Liu, H. L. Dai, L. Wang and F. He, *Appl. Ocean Res.* **88** (2019) 187.
36. M. P. Païdoussis, *Fluid-Structure Interactions: Slender Structures and Axial Flow*, Vol. 1 (Academic Press, 1998).
37. H. Y. Guo and M. Lou, *J. Fluid Struct.* **24** (2008) 496.